Article

Development of a Multi-Segment Parallel Compressor Model for a Boundary Layer Ingesting Fuselage Fan Stage

Jonas Voigt [1,2,*] and Jens Friedrichs [1,2]

1 Cluster of Excellence SE²A—Sustainable and Energy-Efficient Aviation, Technische Universität Braunschweig, 38108 Braunschweig, Germany; j.friedrichs@tu-braunschweig.de
2 Institute of Jet Propulsion and Turbomachinery, Technische Universität Braunschweig, Hermann-Blenk-Straße 37, 38108 Braunschweig, Germany
* Correspondence: j.voigt@ifas.tu-braunschweig.de

Abstract: The present methodological study aims to assess boundary layer ingestion (BLI) as a promising method to improve propulsion efficiency. BLI utilizes the low momentum inflow of the wing or fuselage boundary layer for thrust generation in order to minimize the required propulsive power for a given amount of thrust for wing or fuselage-embedded engines. A multi-segment parallel compressor model (PCM) is developed to calculate the power saving from full annular BLI as occurring at a fuselage tail center-mounted aircraft engine, employing radially subdivided fan characteristics. Applying this methodology, adverse effects on the fan performance due to varying inlet distortions depending on flight operating point as well as upstream boundary layer suction can be taken into account. This marks one step onto a further segmented PCM model for general cases of BLI-induced inlet distortion and allows the evaluation of synergies between combined BLI and active laminar flow control as a drag reduction measure. This study, therefore, presents one further step towards lower fuel consumption and, hence, a lower environmental impact of future transport aircraft.

Keywords: boundary layer ingestion; parallel compressor model; fan performance

1. Introduction

Boundary layer ingestion (BLI) is a promising approach to improve propulsive efficiency in order to increase overall aircraft efficiency [1]. A BLI aircraft configuration consists of engines attached to the wings or the fuselage in a such way that the boundary layer of the aircraft surface is ingested into the propulsor. Due to the resulting lower inflow momentum, the propulsive efficiency is increased. The boundary layer, however, also imposes inhomogeneous inflow conditions to the engine fans. Their impact is to be quantified in order to calculate the overall power saving of BLI.

This study is part of comprehensive efforts to assess the fan reaction to BLI-induced inflow distortions in the scope of overall BLI performance evaluation. Previous studies either used costly CFD simulations, or simplified, averaged engine inflow conditions for that purpose, e.g., [2,3] both considered a Mach number averaged over the concerned boundary layer height to assess the performance of fuselage mounted engines.

The overall goal of the present study is to build a cost-efficient, simplified model based on a parallel compressor model (PCM) that is able to predict the fan efficiency for varying engine dimensions, flight operating points, and inflow conditions, for fast design space exploration. This represents a compromise between accuracy and computational cost compared to inflow averaging or to higher fidelity methods. The present study extends an existing PCM model by introducing radial segmentation, in order to model a fuselage tail fan, which is exposed to a full annular distortion. To the authors knowledge, thus far no studies employing PCM models for fuselage engine performance assessment exist.

The structure of the paper is outlined as follows. First, in Section 2 we introduce the basics of boundary layer ingestion, its advantages and disadvantages, as well as the BLI aircraft design considered in this study. Subsequently, we present parallel compressor modeling in Section 3 and discuss the limitations of that approach. We then outline the radial segmentation approach pursued in the current study. Furthermore, the employed boundary layer data as well as the reference flight scenario are described. Finally, we discuss the resulting fan efficiency and overall BLI power saving.

2. Boundary Layer Ingestion

In the following, we describe the main concept of BLI and a method for BLI power saving quantification.

The thrust F of an idealized jet engine with uniform velocities u and mass-flow $\dot{m}$ can be written as

$$F = \dot{m}_0 \cdot (u_9 - u_0), \tag{1}$$

if the bleed and fuel mass-flow are disregarded. In accordance with the common SAE standard [4], the subscripts 0, 9 refer to the condition upstream of the intake and at the nozzle exit, respectively. The propulsive power P can then be determined by

$$P = \frac{1}{2} \cdot \dot{m}_0 \cdot (u_9^2 - u_0^2). \tag{2}$$

The insertion of Equation (1) into Equation (2) yields a linear dependency from the inflow velocity for the propulsive power, if the thrust and mass flow are considered fixed. This relation is depicted in Figure 1.
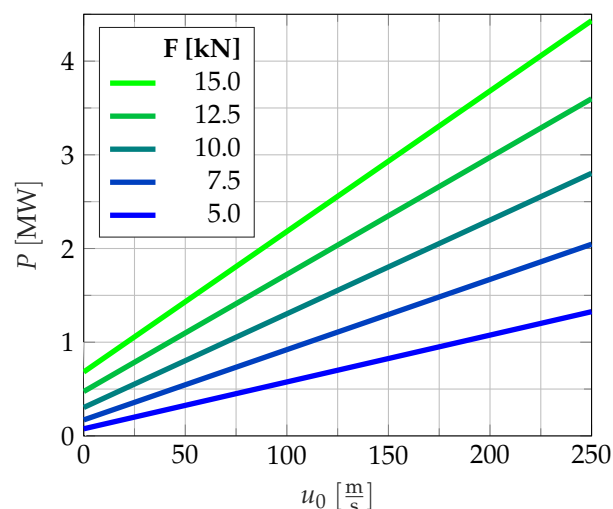

Figure 1. Propulsive power at $\dot{m}_0 = 165\,\mathrm{kg/s}$ for varying thrust requirements.

For a given flight scenario, the power saving due to boundary layer ingestion can be calculated by comparing the BLI engine to a conventional engine fulfilling the same requirements, e.g., delivering the same thrust. We therefore introduce the power saving coefficient (PSC) from [1] as

$$\text{PSC} = \frac{P_{\text{noBLI}} - P_{\text{BLI}}}{P_{\text{noBLI}}}. \tag{3}$$

Engine configurations can also be compared by their thrust specific fuel consumption, which is, at constant thrust, proportional to the difference in absolute total enthalpy over the engine ΔH_t. A corresponding power saving coefficient can be defined as

$$\text{PSC}_{\Delta H_t} = \frac{\Delta H_{t,\text{noBLI}} - \Delta H_{t,\text{BLI}}}{\Delta H_{t,\text{noBLI}}}. \tag{4}$$

As BLI is a novel technology in aviation, its practical implementation is subject to ongoing research. Evaluating the effects is especially difficult, since it features embedding engines with the aircraft structure, making the treatment of complex systems that include interactions between airframe and engines inevitable [5]. In contrary to the explained power saving benefit, BLI also comes with drawbacks.

First, depending on the aircraft and the engine integration concept, BLI introduces an inlet distortion to the fan, resulting in efficiency losses. This is the main subject of this publication and will be discussed in more detail following the next paragraph. Furthermore, in case of asymmetric distortion, the non-uniform inlet flow introduces unsteady blade loading, which can result in additional fan noise due to vibration [6]. Slow boundary layer flow is also more prone to separate in the intake diffusor [7].

On the other hand, when mounting BLI engines on the wings or on a Blended Wing Body fuselage, engine noise is dampened by the aircraft structure [8]. Additionally, it results in a beneficially lower thrust line and reduced weight and drag since no pylon is required and embedded nacelles entail less wetted surface. Furthermore, the same thrust can be archived with smaller engines and nacelles, leading to further weight and drag reduction, in turn smaller required wing area and, therefore, again reduced weight and drag [6,9].

BLI can also be seen as an alternative way to achieve a very low specific thrust without the sizing related challenges that arise from conventional propulsor designs with increasing bypass ratio and nacelle diameter [10].

In Figure 2, asymmetric (Figure 2b) and full annular (Figure 2c) boundary layer ingestion engine concepts are sketched to visualize integration with the aircraft structure and resulting inflow. A conventional podded configuration is drawn for reference (Figure 2a).

In this study, we consider version 2 of the DFG Cluster of Excellence "Sustainable and Energy Efficient Aviation" (SE^{2}A) mid range passenger aircraft, depicted in Figure 3. Its conceptual design is outlined in [11]; for more details refer to Section 4.3. As opposed to a conventional mid-range aircraft with a twin-engine podded configuration, this aircraft features a fuselage tail mounted engine as well as two on-wing engines.
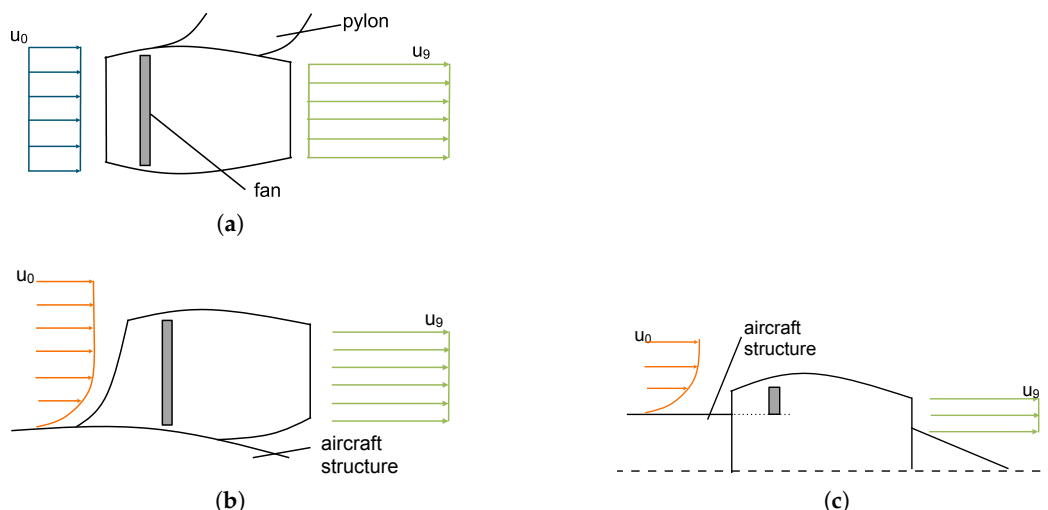

Figure 2. (**a**) Podded vs. (**b**) asymmetric BLI vs. (**c**) full annular BLI engine configuration (Partly based on [12] Figure 5, under CC BY 4.0) (accessed on 25 April 2021).
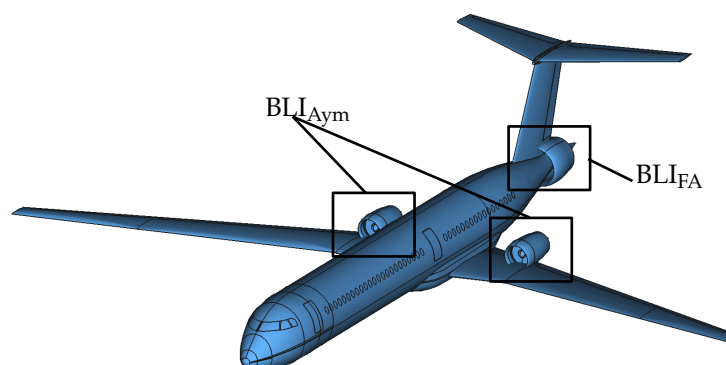
Figure 3. V2 SE^{2}A mid-range aircraft with asymmetric and full annular BLI [11].

While the latter ones are subject to a circumferentially asymmetric inlet distortion (as illustrated in Figure 4a; blue color represents areas of low momentum fluid), the tail engine ingests boundary layer fluid over the full annulus (FA, Figure 4b). This neglects the effect of the T-tail empennage on the inflow conditions and does not consider cross wind conditions or effects from the aircraft angle of attack. According to [10], for commercial transport aircraft, 60% to 70% of drag is of viscous nature. The fuselage is of particular interest for wake filling BLI propulsion because it induces almost half of that portion. If the wings of future aircraft designs are laminarized, that share can rise up to 70% [13]. Two of the four boundary layer cases investigated in the present study also feature large proportions of the fuselage being laminarized, see Section 4.1.
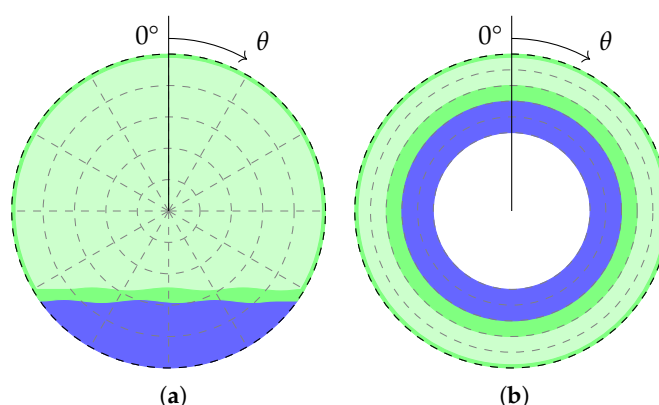
Figure 4. Inflow distortion and PCM segmentation: (**a**) Asymmetric BLI. (**b**) Full annular BLI. Pale green denotes the free stream; blue represents areas of low momentum fluid.

The advantage of a fuselage engine configuration is thus, that high amounts of boundary layer can be ingested with an rotationally symmetric distortion pattern, making an adapted fan design possible do minimize boundary layer induced aerodynamic losses while significantly increasing the propulsive efficiency. Fuselage tail engine concepts are, therefore, subject to various other ongoing research projects, most notably the NASA "STARC-ABL" project, see e.g., [2,14], as well as the Bauhaus Luftfahrt e. V. project "CEN-TRELINE", e.g., [10].

3. Parallel Compressor Model

The basic concept of a parallel compressor model is illustrated in Figure 5. The fundamental idea of the PCM is to split a distorted compressor, here a fan, into two or more sub-compressors that are modeled independently. Each sub-compressor operates over its full face at the local (distorted) conditions, which it represents from the main compressor. The resulting overall operating point and downstream conditions are then defined as the

weighted average of the sub-compressors conditions. A physical quantity ϕ, such as the total-to-total pressure ratio Π_{tt} and the isentropic efficiency $\eta_{s,tt}$, is calculated as

$$\bar{\phi} = \sum_{i=1}^{n} \phi_i \cdot w_i, \tag{5}$$

where w_i represents the weighting of sub-compressor i of n. In a conventional PCM setup, this would represent the angular extend of each sector. ϕ_i is acquired from the undistorted compressor performance map at the distorted inflow conditions. In the case of a BLI-induced distortion, the boundary layer region of lower inflow momentum implies a lower flow coefficient

$$\varphi = \frac{u_m}{u_T} \tag{6}$$

than the undistorted area. The PCM acts as a computationally cost-efficient model to provide an estimate of a distorted turbomachine operating point.
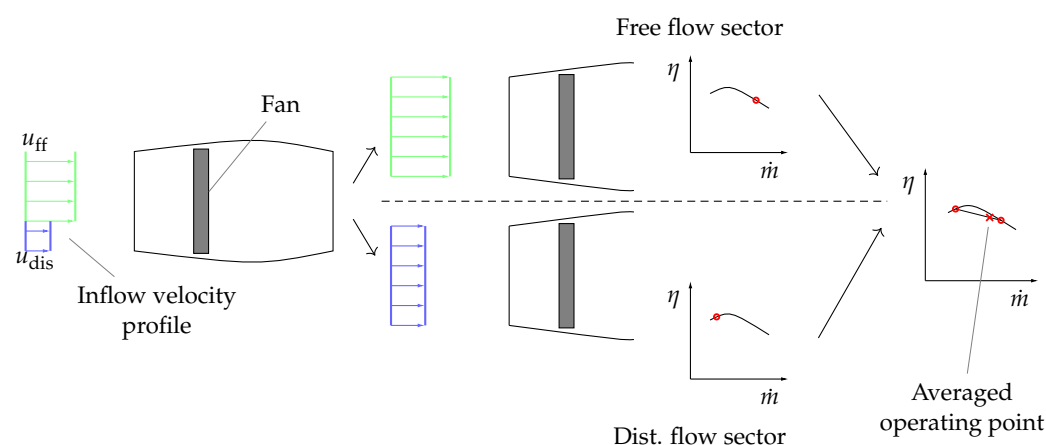
Figure 5. Inflow splitting and basic PCM Scheme (redrawn according to [12] Figure 3, under CC BY 4.0) (accessed on 25 April 2021).

A basic PCM was developed during a previous study [12] to model asymmetric BLI fans by averaging over the boundary layer affected circumferential sector. It was combined with simplified intake and nozzle models and featured a pressure ratio adaption algorithm to calculate the PSC compared to a reference same-thrust free stream engine. Boundary layer data from XFOIL simulations (averaged boundary layer velocity, boundary layer edge velocity, as well as displacement and momentum thickness at a given position on a 2D wing profile representing a Blended Wing Body fuselage) was used to determine the angular extension and the averaged inflow conditions inside one single distorted sector.

The fan exit conditions for the distorted and the undistorted sector were determined from the global stage characteristic at a given rotational speed and averaged to estimate the total pressure ratio and efficiency of the distorted fan. The stage pressure ratio of the fan was then iteratively adapted until it delivered the desired thrust. For further details of the implementation see [12].

This model includes various simplifications that introduce modeling errors. It neglects mass redistribution between the sections of divergent flow conditions and unsteady blade passing effects, as described and mitigated in [15], and is not able to cover the dynamic response of the compression system to unsteadieness in inflow distortions as it is implemented e.g., in the DYNTECC code [16]. Furthermore, inclusion of the inlet swirl is described in [17]. For a comprehensive review of existing approaches in literature to partially mitigate this inaccuracies, see [18].

The basic implementation does not resolve individual blade rows and is, therefore, not able to represent the distorted sector movement over the rotor row [19]. Additionally,

it introduces inaccuracies by (a) averaging the inflow conditions over the whole distortion affected section and (b) not taking the fan characteristics differing over the blade height into account. Those two inadequacies are to be overcome in the present paper and applied to a radially distorted BLI fan in order to estimate the power savings compared to a conventional propulsor configuration.

4. Radially Segmented Parallel Compressor Model

In this section, we describe the extension of the aforementioned PCM to an arbitrary number of radial segments with individual performance characteristics and inflow conditions, which is to be applied to model a fuselage tail engine. This acts as a step towards a general circumferentially and radially segmented PCM, which may then be able to model a variety of distortion configurations. Generating the radial characteristics as well as the applied fuselage boundary layer data is outlined in the following.

4.1. Fuselage Boundary Layer

Multiple boundary layer velocity profiles are considered during this study: A simple flat plate (FP) approach for turbulent flow [20] and data from three different CFD studies carried out with the DLR TAU-Code by [21]. TAU [22] is a finite-volume-based Navier–Stokes solver and was utilized for compressible, steady state calculations on a hybrid mesh. 3D simulations of an axis-symmetric quarter segment of a mid-range aircraft fuselage were conducted for three different configurations. One fully turbulent (FT) simulation was carried out along with two included active laminar flow control (LFC).

The two LFC simulations featured boundary layer suction up to 70% ($LFC_{70\%}$) of the fuselage length and around 50% ($LFC_{50\%}$), respectively. Forced transition was applied slightly downstream the end of the suction area. Studying the combined effect of LFC and BLI is of interest, as boundary layer suction as a drag reduction measure upstream of the engine reduces the degree of boundary layer ingestion, while, at the same time, requiring suction power and implying an additional weight of the suction system.

The development of the boundary layer thickness δ over the fuselage length l is plotted in Figure 6 for all four considered cases. It also features markers for the fuselage positions up onto whom boundary layer suction is applied for the cases $LFC_{70\%}$ and $LFC_{50\%}$.

The boundary layer profiles were evaluated for the marked engine position at 90% fuselage length, equal to $x = 34.2$ m. It can be seen that the flat plate simplification clearly underestimates the boundary layer thickness compared to the fully turbulent CFD calculation. Nevertheless, it is of interest how high the impact of that difference on the PCM models predictions is.

The boundary velocity of the CFD simulations was averaged in the circumferential direction and normalized with the far field velocity u_∞ of the CFD simulations. These are plotted in Figure 7. Normalizing the data, as was similarly performed in [2], was necessary to apply it to different altitude and Mach number conditions, but does introduce modeling inaccuracies.

As can be seen in Figure 7, the flat plate results already highly differ from the fully turbulent CFD simulation. As expected, the upstream boundary layer suction results in less extended near wall areas of low velocity. Due to the conical shape of the rear fuselage (see Figure 6), flow is decelerated, and thus the boundary edge velocity for the CFD cases does not equal the far field velocity at the engine position.
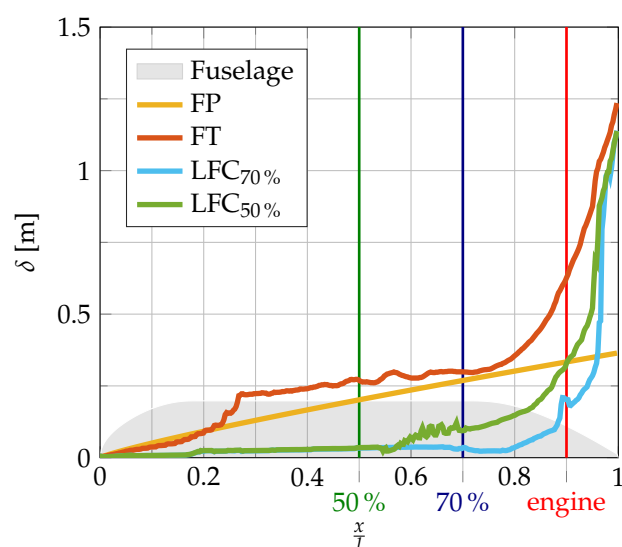
Figure 6. Boundary layer thickness δ over relative fuselage length $\frac{x}{l}$ for the considered cases. Fuselage shape plotted non-proportionally for illustration.
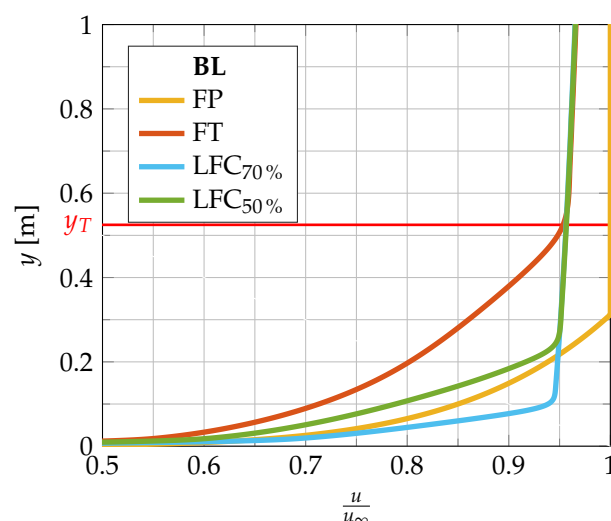

Figure 7. Boundary layer velocity for the considered cases at engine position $x/l = 0.9$ and position y_T of fan tip relative to the wall (see Section 4.3).

4.2. Radial Fan Map

For this study, the Coordinated Research Centre 880 (CRC880) fan stage [23] for the CRC880 engine [24] was considered. This fan stage represents an UHBR design featuring one rotor and one stator row. CFD solutions for the design speed line (3074 /min) from [23] where evaluated over the channel height. They were carried out stationary with the commercial Navier–Stokes solver ANSYS CFX 17.0 on a structured grid, applying the $k - \omega$ turbulence model. A pressure boundary condition was applied at the domain outlet.

Figure 8 depicts the resulting total-to-total pressure ratio $\Pi_{tt} = \frac{p_{t,13}}{p_{t,12}}$ over the stage in radial resolution as well as the isentropic total-to-total efficiency, $\eta_{s,tt} = \frac{a_s}{a}$, plotted over the relative channel height h for the design point. The symbols $p_{t,13}$, $p_{t,12}$ refer to the total pressure up- and downstream of the fan in accordance with [4], while a and a_s denote the real work and the work performed by the hypothetical isentropic reference process.
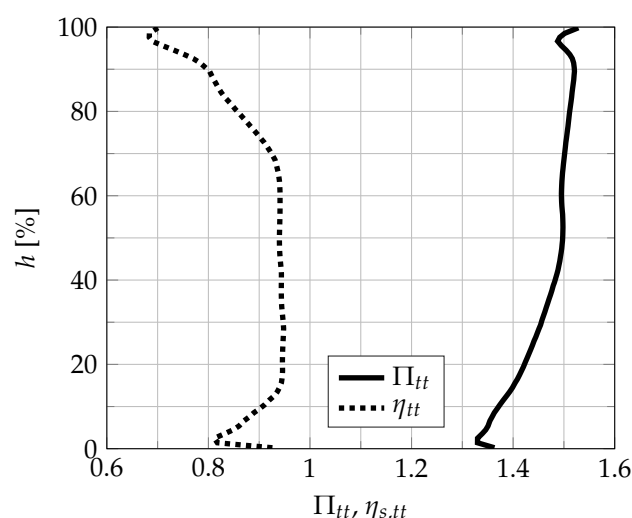
Figure 8. Fan pressure ratio and efficiency over the channel height for the design point.

This radially resolved performance data was then divided into a discrete number n_{RS} of equidistant radial segments. Averaging the segments performance data on each known operating point of the speed line results in radially resolved performance characteristics, as depicted in Figure 9 for a number of five radial segments. The overall stage speed line is plotted for reference. Please note that the number of five segments is chosen for illustrative purposes here, while the results are later generated with ten radial segments, see Section 5.1.
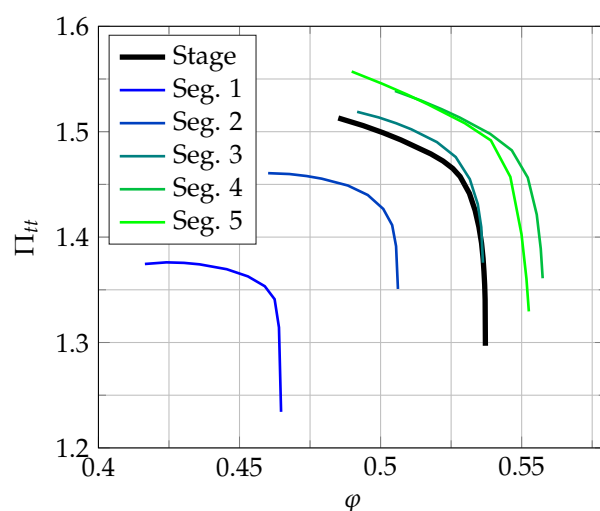
Figure 9. Performance map of the overall fan stage and for each of five radial segments. Counting starts at the hub segment.

The fan map is then scaled in such a way that $h = 0$ is set to the hub radius r_H of a given fan geometry and $h = 1$ at the tip radius r_T, respectively. Note that the fan was not designed for an annular distortion and was not adjusted to these inflow conditions, even though this is possible for a full annular distortion.

The inflow conditions resulting from the fuselage boundary layer are similarly averaged within the defined segments. For a given flight operating point and number of radial segments, this leads to a discrete number i of radial segments, as sketched in Figure 4b for five segments. Each segment has vortex-free, individual inflow conditions

$$\varphi_i = \frac{\bar{u}_{12,i}}{u_T}, \tag{7}$$

a segment-independent total temperature T_t, static pressure p, and density ρ, and individual fan characteristics for constant rotational speed

$$\Pi_{tt,i}, \eta_{s,tt,i} = f_i(\varphi_i) \tag{8}$$

used to determine each operating point $\Pi_{tt,i}, \eta_{s,tt,i}$. This results in the downstream conditions

$$p_{t,13,i} = \Pi_{tt,i} \cdot p_{t,12,i}, \tag{9}$$

and

$$T_{t,13} = T_t \cdot \left(\frac{1}{\eta_{s,tt,i}} \cdot (\Pi_{tt,i}^{\frac{\kappa-1}{\kappa}} - 1) + 1\right) \tag{10}$$

with the isentropic expansion factor $\kappa = 1.4$. Those are averaged following Equation (5), to calculate an overall fan operating point. In addition to the common PCM simplifications described in Section 3, this neglects interactions of the radial segments by independently calculating each radial operating point. The nozzle exit conditions are determined by assuming an adapted nozzle, and subsequently thrust, power propulsive power, and PSCs are calculated from Equations (1)–(4).

4.3. Reference Configuration

The aircraft configuration considered in this study is the V2 SE^{2}A mid range reference aircraft featuring two wings and one tail fuselage engine (Figure 3). The aircraft has a maximum takeoff weight of 69,000 kg, a design range for maximum payload of 3981 km, and 51.57 m wing span with an aspect ratio of 16. For details of the design please refer to [11].

Only cruise is considered in the present study, which leads to an overall thrust requirement of $F_{ac} = 27.72$ kN and a Mach number of $M = 0.78$ m at an altitude of $A = 10,600$ m. The current design phase of the reference aircraft features an equal thrust split between the three engines, leading to a requirement of $F = 9.24$ kN each.

$r_H = 0.3$ m is chosen similar to the dimensions of the tail engine from the NASA STARC-ABL project [14]. Assuming the same specific thrust as the CRC880 engine for seizing leads to an outer diameter of the engine of $r_T = 0.825$ m for the given flight conditions M, A. In Figure 7, $y_T = r_T - r_H = 0.525$ m is plotted to illustrate the position of the fan tip radius relative to the boundary layer velocity profile.

In the following section, the engine dimensions and flight mach number are set to the aforementioned values, while the mentioned values for F and A of the V2 SE^{2}A mid-range aircraft are referred to as the "reference case". If not otherwise mentioned, the fully turbulent CFD boundary layer case is considered.

5. Results

In the this section, we apply the segmented PCM to the reference case and conduct a small parameter variation. The resulting fan efficiency is evaluated as well as its effect on the power saving coefficient.
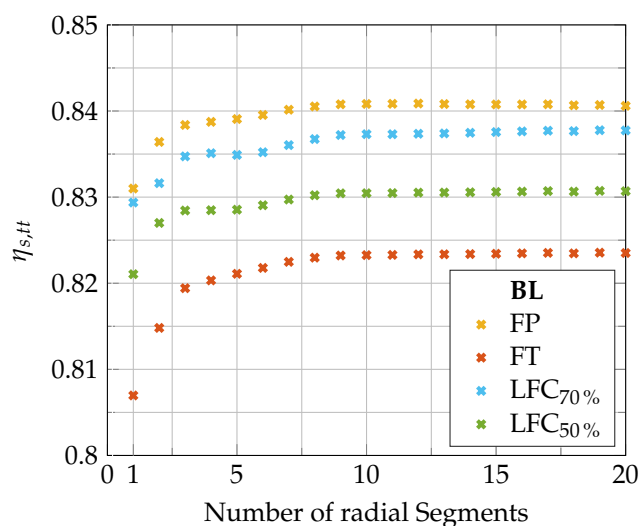
5.1. Convergence Study

First, convergence studies regarding the number of radial segments n_{RS} were conducted in the range from 1 to 20. The results are plotted in Figure 10. Note that $n_{RS} = 1$ is equivalent to averaging inflow conditions over the whole fan face and using the "usual" unsegmented stage fan map.

The study shows good convergence with the radial resolution. The resulting efficiency remains almost constant for $n_{RS} = 10$ and higher; this number of segments is therefore chosen for all following studies.

For a lower n_{RS}, $\eta_{s,tt}$ is comparatively underpredicted. This can be explained by the fact that the mass-specific compression work, as well as the absolute mass-flow per radial increment, is decreasing towards the tip of the fan (see Figure 8). For the current,

not-adapted fan, this outer regions are less affected by the full annular distortion from the fuselage boundary layer, and therefore feature a less reduced local efficiency. The higher the radial resolution, the better this effect is covered.

Figure 10. Convergence study for number of radial segments.

Quantitative values are listed in Table 1. The significant differences between the boundary layer configurations already show the importance of accurately determining the present boundary layer for future studies. Furthermore, the thinner boundary layer in the case of applied LFC leads to reduced efficiency losses due to the decreased distortion.

Table 1. $\eta_{s,tt}$ for varying numbers of radial segments.

| BL Case | n_{RS} | | |
	1	10	20
FP	0.831	0.841	0.841
FT	0.807	0.823	0.824
LFC$_{70\%}$	0.829	0.837	0.838
LFC$_{50\%}$	0.821	0.830	0.831

5.2. Power Saving Coefficient

To quantify the power saving due to BLI, the methodology described in [12] is applied. This includes a simplified model for intake and nozzle. Furthermore, the total pressure ratio of the BLI fan is reduced until the same thrust is archived with the lower inlet momentum and therefore a lower propulsive power requirement. This implies that it is always possible to design a fan of lower pressure ratio with the same efficiency.

In the first step, the BLI engine is compared to a hypothetical undistorted, non-BLI, same-sized engine delivering the same thrust. The results are depicted in Figure 11 for the fully turbulent CFD boundary layer data. Similar to the results of [12], this leads to PSCs decreasing for higher thrusts and higher thrust requirements, while values lay in the order of 2% to 4% for the relevant thrust range.

The influence of the altitude can be explained as follows. As the engine dimensions and Mach number are fixed, the nozzle exit velocity has to increase in order to deliver the same thrust at decreased air density at higher altitudes. The propulsive power requirement is proportional to the difference of the squared inflow and exit velocities. As seen by inserting Equation (2) into (3),

$$\text{PSC} = 1 - \frac{[\dot{m}_0 \cdot (u_9^2 - u_0^2)]_{\text{BLI}}}{[\dot{m}_0 \cdot (u_9^2 - u_0^2)]_{\text{non-BLI}}}, \tag{11}$$

an increase of u_9 for both the BLI and the non-BLI reference case means a decreased influence of the BLI-induced difference in the u_0^2 term and, thus, a decreased PSC. For varying thrust requirements, the mass-flow, inflow conditions, and inflow velocities do not change. Again, the nozzle exit velocity has to be increased to fulfill a higher thrust requirement at a given altitude, leading in turn to lower PSCs. For the reference case R at 10.6 km and 9.24 kN this yields PSC $= 3.38\%$ and $\mathrm{PSC}_{\Delta H_t} = 1.96\%$.
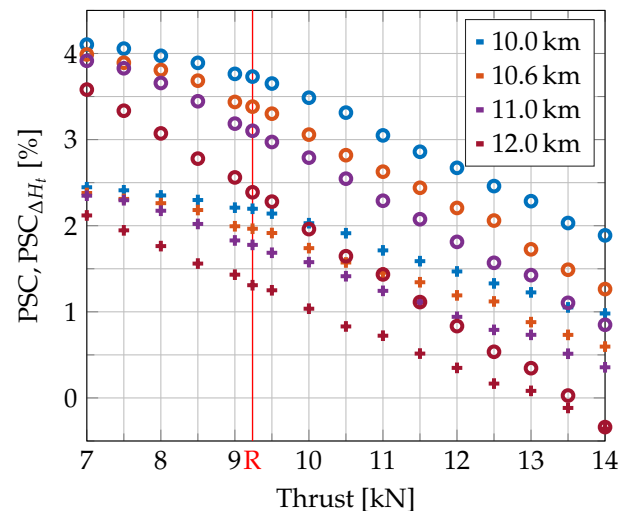
Figure 11. PSC (o) and $\mathrm{PSC}_{\Delta H_t}$ (+) over the thrust requirement for different altitudes for the FT boundary layer.
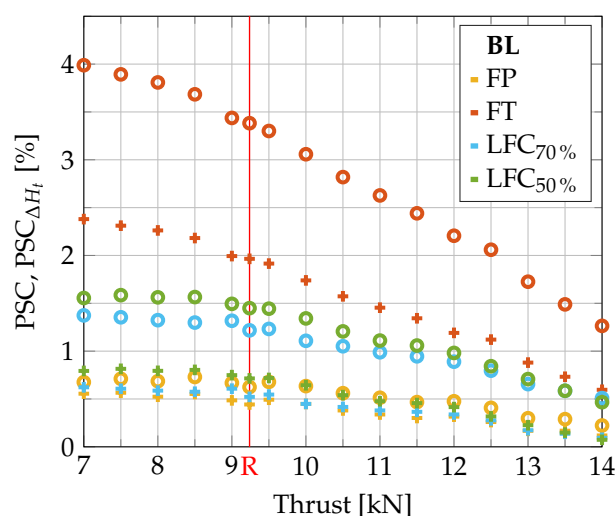
5.3. Varying Boundary Layer Data

When examining the consequences of different boundary layer profiles on the PSC, the values depicted in Figure 12 result. For the reference flight case, they are listed in Table 2 together with the calculated fan efficiency, the propulsive efficiency

$$\eta_a = \frac{F \cdot u_0}{P}, \tag{12}$$

and the product of both. Note that the current model does not consider a core flow, so all power transfer to the fluid is performed by the fan. The two LFC boundary layer profiles, which resulted in less fan losses (compare $\eta_{s,tt}$), generated a significantly lower PSC compared to the case without suction. This means that the increased inflow momentum has a higher negative effect on the overall engine efficiency via the decreased propulsive efficiency than the reduced predicted fan losses due to lower distortion.

This approach can act as one piece of a combined power saving consideration of BLI and LFC. For an overall evaluation, the change in engine thrust requirement due to LFC drag reduction, the required suction power, the momentum of the later expelled suction air, as well as the weight of the suction system need to be taken into account additionally.

Figure 12. PSC (o) and PSC$_{\Delta H_t}$ (+) over the thrust requirement for varying boundary layer conditions at $A = A_{\mathrm{ref}}$.

Table 2. PSC, PSC$_{\Delta H_t}$, and efficiencies for varying boundary layer cases at reference conditions.

BL Case	PSC [%]	PSC$_{\Delta H_t}$ [%]	$\eta_{s,tt}$	η_a	$\eta_{s,tt} \cdot \eta_a$
FP	0.62	0.44	0.841	0.860	0.723
FT	3.38	1.96	0.823	0.910	0.749
LFC$_{70\%}$	1.22	0.52	0.837	0.875	0.733
LFC$_{50\%}$	1.45	0.71	0.830	0.880	0.731

6. Conclusions and Outlook

We presented an implementation of a radially segmented parallel compressor model to describe a distorted fan. The model includes radially resolved fan characteristics and is able to estimate the fans reaction to inflow conditions differing over the channel height. A number of radial segments higher than ten was identified as not further changing the resulting overall operating point.

We applied the model to the fuselage tail engine of a mid range transport aircraft and calculated the power saving coefficient, which is 3.4% for the considered reference case. The fan efficiency as well as the resulting PSC highly depended on the fidelity of the applied boundary layer model and on the presence of upstream boundary layer suction. The accuracy of the employed boundary layer data was, therefore, identified as an essential prerequisite. To derive rules for concurrently applying both BLI and LFC, not only the varying boundary layer patterns but also other parameters and effects of the suction system need to be considered in future studies.

We aim to extend the presented PCM by general circumferential segmentation in following studies and plan to resolve individual blade rows. We intend to conduct the necessary model validation by means of extensive steady and unsteady CFD studies. In the future, the resulting PCM-based model would be able to analyze general symmetric and asymmetric BLI inflow distortions while taking sector movement over the rotor into account.

To obtain reliable quantitative results of the fuselage propulsion power saving, a dedicated, distortion adapted, fuselage fan needs to be designed. This includes adjusting the blade angles to the expected annular distortion. A radially segmented parallel compressor model can be part of that procedure.

Author Contributions: Software, Investigation and Writing, J.V.; Supervision, J.F. Both authors have read and agreed to the published version of the manuscript. All authors have read and agreed to the published version of the manuscript.

Conflicts of Interest: The authors declare no conflict of interest.

Nomenclature

Abbreviations

BL	boundary layer
BLI	boundary layer ingestion
CFD	computational fluid dynamics
CRC	DFG Coordinated Research Centre
DLR	Deutsches Zentrum für Luft- und Raumfahrt e.V.
FP	flat plate (boundary layer case)
FT	fully turbulent (CFD boundary layer case)
LFC	laminar flow control
MR	mid range (aircraft)
PCM	parallel compressor model
PSC	power saving coefficient
R	reference case

Symbols

A	flight altitude
F	thrust
l	fuselage length
h	relative channel height
ΔH	Enthalpy difference
M	Mach number
$\dot{m}$	mass-flow
p	pressure
P	propulsive power
r	radius
T	temperature
u	velocity
w	weighting
x	direction of flow coordinate
y	wall normal coordinate
δ	boundary layer thickness
κ	isentropic expansion factor
η	efficiency
Π	pressure ratio
ϕ	physical output quantity
φ	flow coefficient

Subscripts

0	upstream engine
9	nozzle exit
50 %, 70 %	relative boundary layer suction length
a	propulsive (efficiency)
ac	aircraft
H	fan hub
i	iterator

m	meridional component
n	enumerator
ref	reference
RS	radial segments
s	isentropic
t	total
T	fan tip
tt	total-to-total
∞	far-field

References

1. Smith, L.H. Wake Ingestion Propulsion Benefit. *J. Propuls. Power* **1993**, *9*, 74–82. [CrossRef]
2. Welstead, J.; Felder, J.L. Conceptual Design of a Single-Aisle Turboelectric Commercial Transport with Fuselage Boundary Layer Ingestion. In Proceedings of the 54th AIAA Aerospace Sciences Meeting, San Diego, CA, USA, 4–8 January 2016; AIAA SciTech Forum; American Institute of Aeronautics and Astronautics: Reston, VA, USA, 2016. [CrossRef]
3. Bijewitz, J.R. Conceptual Sizing Methods for Propulsive Fuselage Aircraft Concepts. Ph.D. Thesis, Technische Universität München, München, Germany, 2020.
4. SAE International. *ARP755: Aircraft Propulsion System Performance Station Designation and Nomenclature*; Technical Report; SAE International: Warrendale, PA, USA, 1991.
5. Uranga, A.; Drela, M.; Greitzer, E.M.; Hall, D.K.; Titchener, N.A.; Lieu, M.K.; Siu, N.M.; Casses, C.; Huang, A.C.; Gatlin, G.M.; et al. Boundary Layer Ingestion Benefit of the D8 Transport Aircraft. *AIAA J.* **2017**, *55*, 3693–3708. [CrossRef]
6. Dowling, A.P.; Hynes, T. Towards a Silent Aircraft. *Aeronaut. J.* **2006**, *110*, 487–494. [CrossRef]
7. Rodriguez, D.L. A Multidisciplinary Optimization Method for Designing Boundary Layer Ingesting Inlets. Ph.D. Thesis, Stanford University, Atlanta, GA, USA, 2002.
8. Campbell, R.; Carter, M.; Pendergraft, O.; Friedman, D.; Serrano, L. Design and Testing of a Blended Wing Body with Boundary Layer Ingestion Nacelles at High Reynolds Numbers. In Proceedings of the 43rd AIAA Aerospace Sciences Meeting and Exhibit, Reno, NV, USA, 10–13 January 2005; p. 459.
9. Uranga, A.; Drela, M.; Hall, D.K.; Greitzer, E.M. Analysis of the Aerodynamic Benefit from Boundary Layer Ingestion for Transport Aircraft. *AIAA J.* **2018**, *56*, 4271–4281. [CrossRef]
10. Seitz, A.; Habermann, A.L.; Peter, F.; Troeltsch, F.; Castillo Pardo, A.; Della Corte, B.; van Sluis, M.; Goraj, Z.; Kowalski, M.; Zhao, X.; et al. Proof of Concept Study for Fuselage Boundary Layer Ingesting Propulsion. *Aerospace* **2021**, *8*, 16. [CrossRef]
11. Karpuk, S.; Elham, A. Conceptual Design Trade Study for an Energy-Efficient Mid-Range Aircraft with Novel Technologies. In Proceedings of the AIAA Scitech 2021 Forum, Nashville, TN, USA, 11–15 January 2021; American Institute of Aeronautics and Astronautics: Reston, VA, USA, 2021. [CrossRef]
12. Budziszewski, N.; Friedrichs, J. Modelling of A Boundary Layer Ingesting Propulsor. *Energies* **2018**, *11*, 708. [CrossRef]
13. Steiner, H.J.; Seitz, A.; Wieczorek, K.; Plötner, K.; Isikveren, A.T.; Hornung, M. Multi-Disciplinary Design and Feasibility Study of Distributed Propulsion Systems. In Proceedings of the 28th International Congress of the Aeronautical Sciences, Brisbane, Australia, 23–28 September 2012; pp. 23–28.
14. Lee, B.J.; Liou, M.F.; Liou, M.S. Conceptual Aerodynamic Design of a Tail-Cone Thruster System Under Axi-Symmetric Inlet Distortion. In Proceedings of the ASME Turbo Expo 2018: Turbomachinery Technical Conference and Exposition, Oslo, Norway, 11–15 June 2018; American Society of Mechanical Engineers Digital Collection: New York, NY, USA, 2018. [CrossRef]
15. Shahrokhi, K.; Milt Davis, J. Application of a Modified Dynamic Compression System Model to a Low Aspect Ratio Fan—Effects of Inlet Distortion. In Proceedings of the 33rd Aerospace Sciences Meeting and Exhibit, Reno, NV, USA, 9–12 January 1995; American Institute of Aeronautics and Astronautics: Reston, VA, USA, 1995. [CrossRef]
16. Hale, A.; Davis, M. DYNamic Turbine Engine Compressor Code (DYNTECC)—Theory and Capabilities. In Proceedings of the 28th Joint Propulsion Conference and Exhibit, Nashville, TN, USA, 6–8 July 1992; American Institute of Aeronautics and Astronautics: Reston, VA, USA, 1992. [CrossRef]
17. Davis, M.W.; Cousins, W.T. Evaluating Complex Inlet Distortion With a Parallel Compressor Model: Part 2—Applications to Complex Patterns. In Proceedings of the ASME 2011 Turbo Expo: Turbine Technical Conference and Exposition, Vancouver, BC, Canada, 6–10 June 2011; American Society of Mechanical Engineers Digital Collection: New York, NY, USA, 2012; pp. 13–23. [CrossRef]
18. Cousins, W.T.; Davis, M.W. Evaluating Complex Inlet Distortion With a Parallel Compressor Model: Part 1—Concepts, Theory, Extensions, and Limitations. In Proceedings of the ASME 2011 Turbo Expo: Turbine Technical Conference and Exposition, Vancouver, BC, Canada, 6–10 June 2011; American Society of Mechanical Engineers Digital Collection: New York, NY, USA, 2012; pp. 1–12. [CrossRef]
19. Mazzawy, R.S. Multiple Segment Parallel Compressor Model for Circumferential Flow Distortion. *J. Eng. Power* **1977**, *99*, 288–296. [CrossRef]
20. Truckenbrodt, E. *Lehrbuch der Angewandten Fluidmechanik*; Springer: Berlin/Heidelberg, Germany; New York, NY, USA; Tokyo, Japan, 1983.

21. Beck, N.; Landa, T.; Seitz, A.; Boermans, L.; Liu, Y.; Radespiel, R. Drag Reduction by Laminar Flow Control. *Energies* **2018**, *11*, 252. [CrossRef]
22. Schwamborn, D.; Gerhold, T.; Heinrich, R. The DLR TAU-Code: Recent Applications in Research and Industry. In Proceedings of the European Conference on Computational Fluid Dynamics, Egmond aan Zee, The Netherlands, 5–8 September 2006; p. 25.
23. Giesecke, D.; Friedrichs, J.; Stark, U. Preliminary Aerodynamic Design of a Fan Stage for an Ultra High Bypass Ratio Engine. In Proceedings of the ISABE 2017—23rd ISABE Conference, Mancester, UK, 3–8 September 2017; p. 16.
24. Giesecke, D.; Lehmler, M.; Friedrichs, J.; Blinstrub, J.; Bertsch, L.; Heinze, W. Evaluation of Ultra-High Bypass Ratio Engines for an over-Wing Aircraft Configuration. *J. Glob. Power Propuls. Soc.* **2018**, *2*, 493–515. [CrossRef]